scienceOPENresearch SOR-CHEM

The spherical nucleic acids mRNA detection paradox

David Mason[1,2], Gemma Carolan[2], Marie Held[2], Joan Comenge[2], and Raphaël Lévy[*2]

[1]Centre for Cell Imaging, Institute of Integrative Biology, University of Liverpool, Biosciences Building, Crown Street, Liverpool L69 7ZB, UK
[2]Department of Biochemistry, Institute of Integrative Biology, University of Liverpool, Biosciences Building, Crown Street, Liverpool L69 7ZB, UK
*Corresponding author's e-mail address: rapha@liverpool.ac.uk

Published online: 17 November 2015 (version 1)
Cite as: Mason et al. ScienceOpen Research 2015 (DOI: 10.14293/S2199-1006.1.SOR-CHEM.AZ1MJU.v1)
Reviewing status: Please note that this article is under continuous review. For the current reviewing status and the latest referee's comments please click **here** or scan the QR code at the end of this article.

Primary discipline: Chemistry
Secondary discipline: Life sciences
Keywords: Gold nanoparticles, Smartflare, Nano-flare, Sticky-flare, Endosomal escape, Biological barriers, Open science, Live cell imaging, mRNA detection, Intracellular sensing

ABSTRACT

From the 1950s onwards, our understanding of the formation and intracellular trafficking of membrane vesicles was informed by experiments in which cells were exposed to gold nanoparticles and their uptake and localisation, studied by electron microscopy. In the last decade, building on progress in the synthesis of gold nanoparticles and their controlled functionalisation with a large variety of biomolecules (DNA, peptides, polysaccharides), new applications have been proposed, including the imaging and sensing of intracellular events. Yet, as already demonstrated in the 1950s, uptake of nanoparticles results in confinement within an intracellular vesicle which in principle should preclude sensing of cytosolic events. To study this apparent paradox, we focus on a commercially available nanoparticle probe that detects mRNA through the release of a fluorescently labelled oligonucleotide (unquenching the fluorescence) in the presence of the target mRNA. Using electron, fluorescence and photothermal microscopy, we show that the probes remain in endocytic compartments and that they do not report on mRNA level. We suggest that the validation of any nanoparticle-based probes for intracellular sensing should include a quantitative and thorough demonstration that the probes can reach the cytosolic compartment.

The history of gold nanoparticles as tools for biological research and medical diagnostics starts more than a century ago. In 1912, Carl Friedrich August Lange invented a nanoparticle-based test to diagnose *dementia paralytica*. The test was based on colour change upon aggregation induced by non-specific interactions with proteins from the spinal fluids of patients [1]. For several decades, the test was used in clinics and its existence spurred synthetic efforts towards better nanoparticle preparations [2]. With the development of electron microscopy in the 1940s and 1950s, gold nanoparticles became contrast agents of choice due to their high electron density, favourable dimensions and relative ease to prepare antibody conjugates. Some of the earliest studies of vesicular trafficking used gold colloids as electron microscopy probes. In 1957, Harford et al. exposed HeLa cells to gold nanoparticles, observed localisation within intracellular vesicles by electron microscopy and concluded that their results supported the notion that *membranous organelles of the cytoplasm may be derived from the cell membrane* [3]. Thus, nanoparticles have been one of the early tools that biologists have used to decipher the way cells probe their environment. They were also used as a proxy to study the entry of biological nanoparticles, i.e. viruses, into cells. As early as 1965, it was noted in an elegant side-by-side electron microscopy study that while the Herpes viral particles escape endosomes, gold colloids remain in vesicles after uptake [4]. Indeed virions, being under a selective reproductive pressure, have evolved advanced means by which to escape their encapsulating vesicle and access the cytosol (for example, adenovirus [5]). Thus, more than five decades of work has clearly established that nanoparticles enter cells by endocytotic mechanisms that result in their entrapment inside intracellular vesicles unless those nanoparticles are biological in nature and have acquired through evolution, advanced molecular tools which enable them to escape. Access to the cytosol remains one of the main barriers towards biologics and siRNA therapeutic application [6–9]. For cell biology experiments, access to the cytosol can be gained through disruptive physical means such as electroporation or endosomal rupture through the use of osmotic pressure[10], liposome carriers or the proton sponge effect [11]. For purposes such as transfection, it is often acceptable that most particles remain trapped in endosomes as long as a few particles per cell reach the cell machinery.

From the first decade of this century, the number of publications reporting the interaction and uptake of nanoparticles in cells has exploded, often ignoring the knowledge gained from these earlier experiments. The previously mentioned Harford *et al*. study [3] has been cited five times since 2000; in the same period over 5,000 articles were published on the topic of gold nanoparticles and their interaction with cells, with the number of articles nearly doubling every two years since 2007 (Web of Knowledge search for topic: "gold nanoparticle*" and "cell" and "uptake or entry or penetration or endocytosis"). In spite of endosomal entrapment, nanoparticles have been proposed for intracellular sensing within the cytosol of live cells, including the detection of caspase three activity by plasmon rulers [12] and the regulation, quantification and imaging of specific mRNAs with spherical nucleic acids [13–16]. The interpretation of such experiments relies on the particles being in the correct compartment. For imaging and sensing purposes, retention of the majority of the particles in endosomes would lead to incorrect conclusions. Unfortunately, direct evidence of endosomal escape is lacking in these studies.

RNA plays a central role in the conversion of DNA into proteins in cells. More than just a genetic translator, these highly specialised molecules play an active and highly dynamic role in gene expression, promoting silencing, up-regulation or modification of translation. Present studies on RNA are largely restricted to fixed or *in vitro* methods such as fluorescent *in situ* hybridisation, RT-PCR and gel electrophoresis. Fluorescent reporters that could get live, dynamic measurements of mRNA within cells or tissues would therefore have an enormous potential to improve our understanding of biology. The spherical nucleic acid gold nanoparticles developed by the Mirkin lab for detection of mRNA are commercially available from EMD Merck Millipore under the name SmartFlares. The technology relies on the hybridisation of target mRNA strands with complementary strands which are covalently linked to a gold nanoparticle. Upon hybridisation a fluorescent reporter strand is displaced, and subsequently un-quenched when no longer in the vicinity of the gold core, providing a readout of mRNA levels. A more recent implementation (named StickyFlares) relies on the same technology but inverts the sequences such that the fluorescent reporter strand is complementary to the mRNA of interest [15].

Given the limited amount of published information on the endosomal escape of spherical nucleic acids, we have studied the localisation of their commercially available form, i.e. SmartFlares. We have carried this research as an open science project, sharing our data and protocols in quasi-real time using an online notebook [17] and data repository [18]. This has allowed us to gather feedback from peers including other SmartFlare users and developers. Using high-resolution fluorescence microscopy, electron microscopy and photothermal imaging we have found that using the manufacturers' instructions, the SmartFlares are taken up into vesicular compartments in a subset of cells. We find that after 16–20 h, fluorescence is present and remains visible as puncta within membrane-contained vesicles. Importantly, the fluorescence levels are independent of the presence of the target mRNA. Given these findings, we suggest that the validation of any nanoparticle-based probes for intracellular sensing should include a quantitative and thorough demonstration that the probes can reach the cytosolic compartment.

MATERIALS AND METHODS

Materials

SmartFlare mRNA detection probes were ordered from EMD Merck Millipore. Uptake and Scrambled controls were Cy5-labelled while vascular endothelial growth factor (VEGF) SmartFlares were Cy3-labelled. SmartFlares were re-suspended in 1-mL nuclease-free de-ionised water and stored at room temperature protected from light according to the manufacturer's instructions.

Fluorescein isothiocyanate (FITC)-labelled 10-kDa dextran (from Life Technologies – now ThermoFisher Scientific) was re-suspended to 10 mg mL^{-1} in phosphate-buffered saline (PBS). Dimethyloxaloylglycine (DMOG), Triton X-100 and bovine serum albumin (BSA) were from Sigma Aldrich. DMOG stocks were used within 2 months of reconstitution and aliquoting into −20°C. All cell culture media were from Gibco (now ThermoFisher Scientific).

Primary antibodies were purchased from Abcam against LAMP1 (AB24170) and Transferrin Receptor (AB84036). Secondary antibodies were purchased from Life Technologies (now ThermoFisher Scientific) conjugated with AlexaFluor 488 (A11008), 568 (A11011) or 647 (A21244) as required.

HeLa cells (ATCC) were grown in 10-cm dishes (Corning) and split into 35-mm glass-bottomed dished (Ibidi) for experiments.

Cell culture

HeLa cells were maintained in Dubecco's modified essential medium growth media supplemented with 10% foetal bovine serum, 1% non-essential amino acids and 1% penicillin/streptomycin. Cells were maintained between 20% and 80% confluent at 37°C and 5% CO_2.

mRNA detection experiments

The SmartFlare RNA detection probes were used as directed by the manufacturer. Briefly, ~400,000 HeLa cells were seeded onto 35-mm glass-bottomed imaging dishes and incubated in growth media for 6 h to adhere. Media were pre-mixed by aliquoting (per well) 960 μL of media, 20 μL of SmartFlare stock solution and 20 μL of fluorescent dextran (10 mg mL^{-1} stock). In experiments with other drugs they were included at noted concentrations and the volume of media reduced accordingly to compensate. Growth media

were replaced with the above mixture and the cells returned to the incubator for 18 h or as noted.

Confocal microscopy

Fluorescent imaging was conducted at the Centre for Cell Imaging in Liverpool using a Zeiss LSM510 multiphoton microscope. Where possible, multipass dichroic mirrors and filters were used to reduce the potential for spatial misalignment. In all experiments, the confocal pinhole was adjusted to maintain a similar optical slice between channels. For live experiments, incubation and CO_2 control maintained environmental conditions as in *Cell Culture* above. Unless otherwise stated, all fluorescent images are shown without any contrast enhancement.

Electron microscopy

Cells were fixed with a solution containing 1% paraformaldehyde and 3% gluteraldehyde in 0.1-M cacodylate buffer (pH 7.4). They were stained first with reduced osmium (2% OsO4 + 1.5% K4[Fe(CN)6]). This was followed by a second osmium staining (2% OsO4) and a uranyl acetate (1%) staining. Samples were then dehydrated in graded ethanol (30%, 50%, 70%, 90% and twice 100%). Finally, samples were infiltrated with resin (product number 812 from TAAB Microscopy Supplies) and embedded with the same resin. The resin was cured for 48 h at 60°C. Ultrathin sections of 350 μm × 350 μm × 74 nm were cut and placed in 200 mesh formvar/carbon filmed grids. They were post-stained with uranyl acetate and lead citrate before imaging on a Tecnai G3 spirit.

Photothermal microscopy

Cells were fixed in 4% Paraformaldehyde (PFA) for 20 min at room temperature. Subsequently, the cells were washed with PBS and immersed under 2 mL of PBS + 0.01% sodium azide for storage at 4°C between imaging sessions.

All images were acquired using a custom photothermal microscope [19] built around the body of a Nikon Eclipse Ti-U inverted microscope. Prior to photothermal imaging, the samples were allowed to equilibrate fully to room temperature for at least an hour. Fluorescence images were recorded using an X-Cite Series 120 light source (now Excelitas Technologies, USA) together with an FITC filter set for the Dextran signal and Cy5 filter set for the SmartFlare signal immediately prior to photothermal imaging.

The photothermal excitation laser (523 nm, 0.5 mW; frequency-doubled Nd:YAG, Ventus Laser Quantum, Germany) was modulated at a frequency of 459.5 kHz using an accousto-optical modulator (Isomet Corporation, UK). The excitation beam was overlaid with a non-resonant probe laser (633 nm, 1.0 mW; JDS Uniphase Corporation, USA) via a cold mirror (ThorLabs, USA). The superimposed beams were focused onto the sample via a Zeiss Plan Achromat 63× oil immersion objective (numerical aperture: 1.4). The sample was placed on a piezo scanning stage (MCL502385, MadCity Labs, USA), which allows the movement of the sample in three dimensions over the fixed laser spot. Pixel-by-pixel scanning was facilitated by a piezoelectric stage driver (MCL NanoDrive 85, MadCity Labs, USA) controlled through a Nanonis RC4 module and Nanonis program (SPECS Zurich, Switzerland). The transmitted and forward scattered light was collected via a Zeiss Achroplan 40× water immersion objective (numerical aperture: 0.8) and passed through a red-pass filter (ThorLabs, USA) to block the excitation laser. The red component was focused on a photodiode of the balanced photo receiver (Model 2107 10 MHz adjustable photo receiver, New Focus, USA). A lock-in amplifier (DSP 7260, Signal Recovery, USA) was used to identify the scattered component of the probe beam that corresponds to the modulation frequency (i.e. 459.5 kHz). A Nanonis SC4 Acquisition Module (SPECS Zurich, Switzerland) was used for signal acquisition. The signal was averaged and a greyscale pixel value was generated. The pixel-by-pixel values were then converted into a photothermal image and saved in the Nanonis-native .sxm format.

Immunofluorescence

Cells were treated identically as to the "*mRNA detection experiments*" above; however, instead of imaging the samples live, they were washed once in PBS and then fixed in 4% PFA for 20 min at room temperature. Subsequently, samples were washed at least once with PBS to remove excess fixative then blocked and permeabilised using 0.1% TritonX-100 plus 1% BSA in PBS for 60 min at room temperature. Samples were washing three times with PBS. Primary antibodies were diluted in 1% BSA in PBS at 1:500 and added to the samples for 60 min at room temperature. Samples were washed three times for 15 min each in PBS, then secondary antibodies were added at 1:1000 dilution in 1% BSA in PBS for 60 min at room temperature. Cells were washed three times in PBS then imaged immediately or stored under 2 mL of PBS + 0.01% sodium azide at 4°C for later imaging.

Data analysis

All data analyses were performed using the Open Source Fiji (available from http://fiji.sc). As shown in Figure 1, estimates of particle size were made on calibrated images by thresholding the electron dense particles by intensity, followed by the application of a 2D watershed filter to split separating objects. The analysed particles function was used to report the minimum and maximum Feret diameters of particles with an area greater than 100 nm^2 with circularity greater than 0.7 (to exclude amorphous bunches of particles). For each particle, the mean of the maximum and minimum Feret diameter was calculated. The population mean is reported.

As shown in Figure 3, the change in intensity after DMOG treatment was measured by background subtracted raw integrated density for a field of cells and dividing this by the

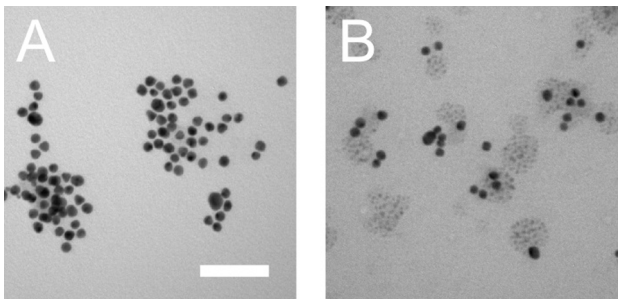

Figure 1. Physical characterisation of SmartFlare RNA detection probes: SmartFlares were re-suspended in nuclease-free deionised water and 10 µL dried onto formvar/carbon electron microscopy grids. Samples of the uptake control (A) and VEGF SmartFlares (B) were imaged on a technai spirit transmision electron microscope (TEM) at a nominal magnification of 150,000 times. The scale bar represents 100 nm.

number of cells in the field. Within experimental repeats, the data were normalised to an untreated control, and the mean of these values was reported. The results of three experiments (each with eight-fields) were analysed in this way. A two-tailed heteroscedastic Student's *t*-test was used to assess significance ($P = 0.065$).

As shown in Figure 4, the SmartFlare fluorescence channel was compared to a second channel and analysed using the JaCoP plugin for Fiji [20], for colocalisation using a thresholded Manders' analysis. Given the non-homogeneous uptake of SmartFlares by cells, the values reported are the coefficient relating to the overlap between SmartFlares and the secondary label.

Open science

This project has been run as an Open Science project, with results, thoughts, commentary and discussion posted at [http://raphazlabcommons.wordpress.com]. The raw data were both managed internally and made available, through the OMERO server at the Liverpool Centre for Cell Imaging. We would like to acknowledge the help of the Open Microscopy Environment group (University of Dundee), specifically Will Moore, for help with developing our public-facing gallery hosted at [http://cci02.liv.ac.uk/gallery].

RESULTS AND DISCUSSION

Characterisation of SmartFlare RNA detection probes

As an exemplar target, we chose the VEGF because it is present in all mammalian cells, its regulation is relevant to a range of diseases and its expression level can be manipulated pharmacologically with dimethyloxalylglycine (DMOG) [21,22].

As gold nanoparticles have a known propensity to aggregate and agglomerate, we sought to first characterise the VEGF SmartFlares along with the "Uptake Control". Transmission electron microscopy (TEM) showed no apparent aggregation (Figure 1A and B) of the particles and allowed a measurement of the particle diameters (VEGF: 16 nm, SD = 2.34 nm, $n = 310$ particles; uptake control: 14 nm, SD = 1.82 nm, $n = 93$ particles), which compared well to the expected diameter of 13 nm.

SmartFlares are taken up into cells

Following the manufacturers' instructions, Uptake Control SmartFlares were added to HeLa cells and incubated for 18 h. Live-cell imaging with a laser-scanning confocal microscope revealed fluorescent puncta of ~1 µm diameter in approximately a quarter of the cells, with the intensity of the puncta varying between individual puncta and also between cells (Figure 2A–C). Both the VEGF and Scrambled SmartFlares showed a very similar punctate distribution within the cell. This was unexpected for two main reasons. First, SmartFlares are sold on the basis of being able to escape the endosomes in order to interact with RNA in the cytosol [23,24]. Second, in order to become fluorescent, the SmartFlares are ostensibly required to interact with target RNA molecules, of which we would expect limited amounts within endocytic vesicles.

SmartFlares remain in vesicles up to 18 h

The punctate distribution as can be seen in Figure 2 could result from aggregation in the cytosol, vesicular containment or binding to the surface of cells. In order to examine this at higher resolution, SmartFlare-loaded cells were imaged using TEM. From an initial screen of the EM grid studying at least 20 cells, gold particles were only seen to be contained within membrane-bound compartments (Figure 3A and B). Some sections did not present any gold nanoparticles.

The TEM data show that the SmartFlares are contained within membrane-bound compartments. To test whether their fluorescence is nevertheless sensitive to the levels of VEGF mRNA, cells were treated at the time of SmartFlare addition, with DMOG, a drug known to up-regulate VEGF mRNA levels by 10 times over this time course [25]. As shown in Figure 3C–E, however, DMOG treatment did not affect the intensity of the VEGF SmartFlare signal.

To evaluate the respective localisation of the gold core and unquenched fluorescence reporter, we combined fluorescence and photothermal microscopy to visualise the gold core and fluorescent dye in the same sample. This showed the fluorescent puncta and nanoparticles to be within the same compartments (Figure 3F–H).

Characterisation of the SmartFlare-containing vesicles

Having confirmed that the SmartFlares were membrane-bound, we set about trying to characterise the SmartFlare-containing compartments. There are several ways in which

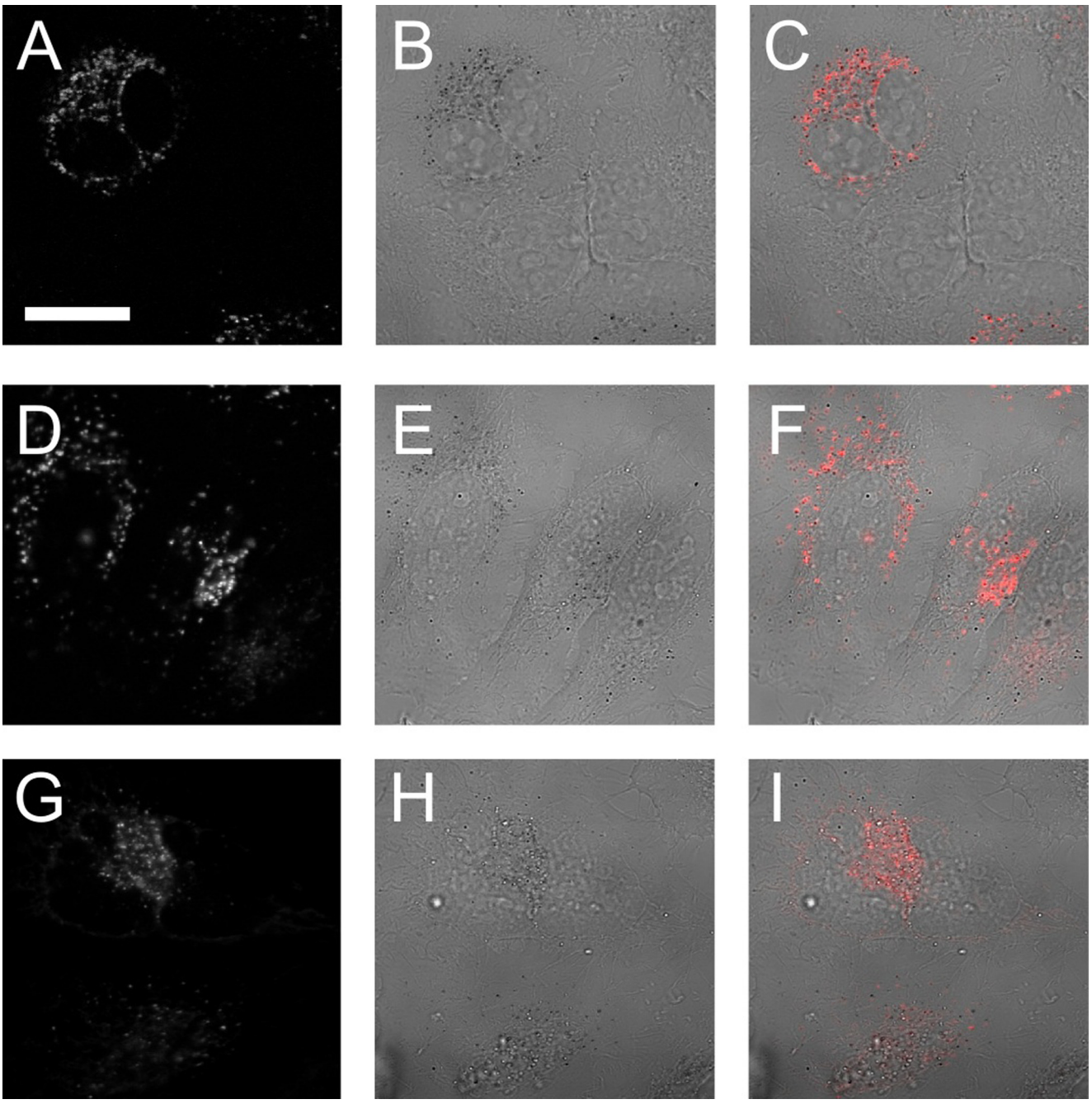

Figure 2. Cellular uptake of SmartFlares: HeLa cells were exposed to uptake control (A–C), VEGF (D and E) or scrambled control (G–I) SmartFlares for 18 h, then washed and imaged with confocal laser-scanning microscopy in fluorescence (A, D and G) or transmitted (B, E and H) channels. An overlay of the two channels is shown in C, F and I. All frames are shown at identical magnification, scale bar represents 10 μm.

material impermeant to the cell membrane can be taken up into cells. Endocytosis is probably the most well-studied category and is largely driven by receptor-mediated signalling, whereas pinocytic processes are considered constitutive and are responsible for fluid-phase (IE receptor independent) uptake. The terminal compartment of these processes is the lysosome, a highly nucleolytic and proteolytic compartment involved in degradation and in some cells, antigen presentation.

We labelled the endocytic pathway using a fluorescently labelled 10-kDa dextran, both to show that constitutive uptake was occurring in our system, but also to label all of the compartments of the pathway. As expected, the dextran labelled every cell in the field with homogeneous intensity

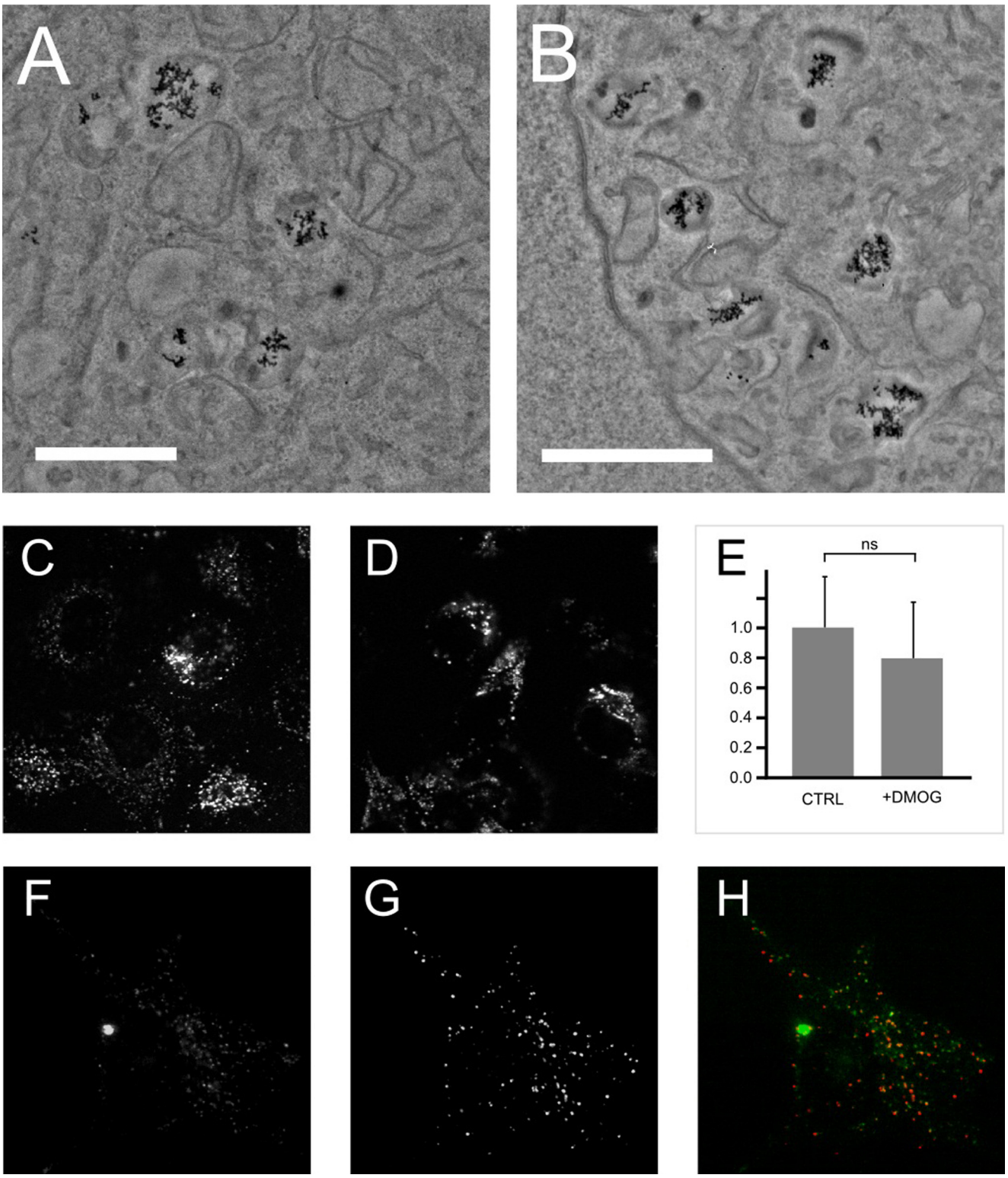

Figure 3. Confirming vesicular containment of SmartFlares: HeLa cells were loaded with uptake control (A) or VEGF (B) SmartFlares for 18 h then prepared for TEM as detailed in the *Materials and Methods* section. Scale bars represent 1000 nm. Confocal microscopy was used to study VEGF SmartFlare-loaded control (C) and DMOG-treated cells (D). No increase in intensity was observed in three independent experiments (E). Correlative fluorescence (F) and photothermal (G) microscopy were used to view SmartFlare fluorescence and gold nanoparticle cores in the same sample.

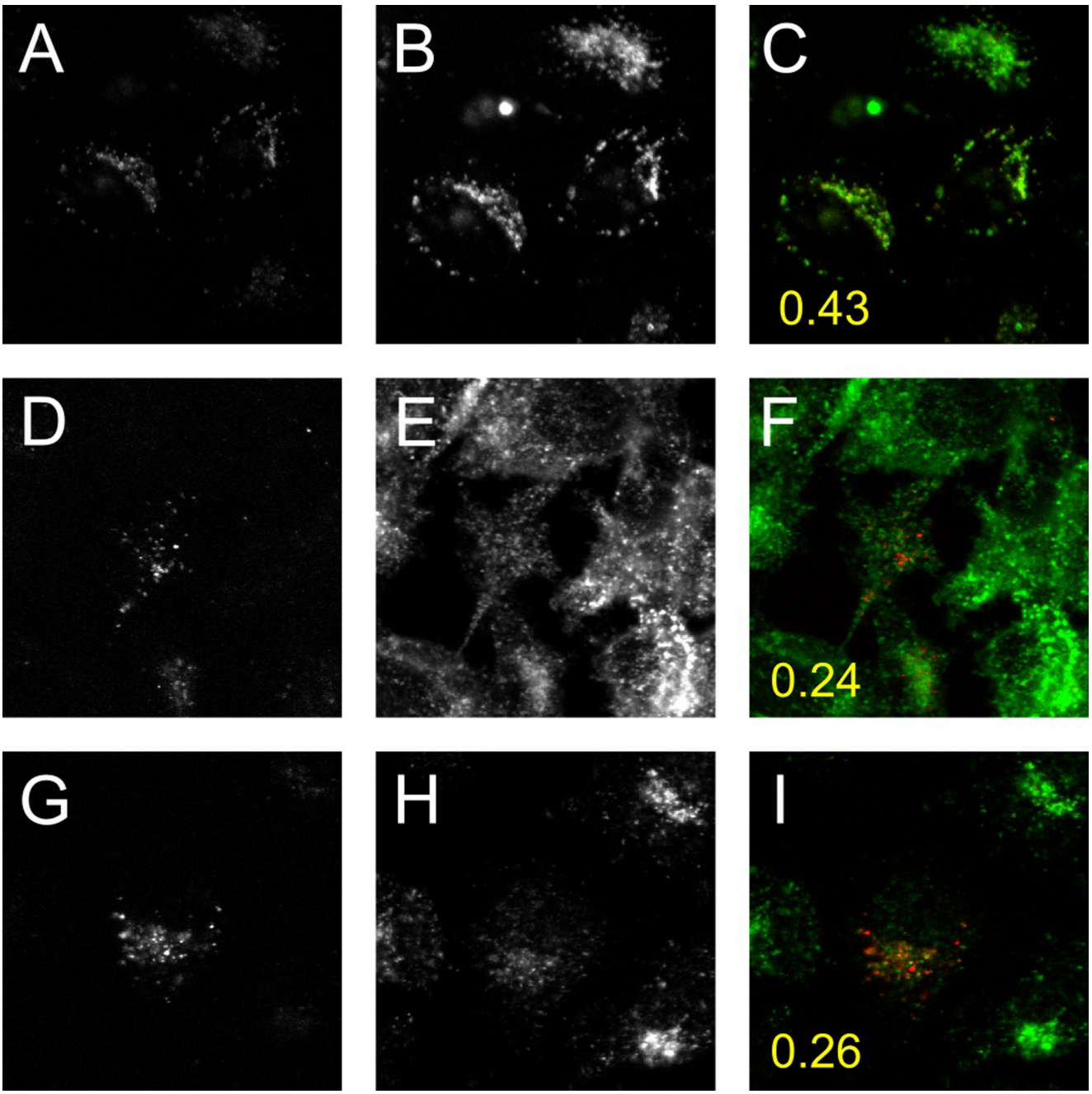

Figure 4. Studying the localisation of SmartFlares: HeLa cells were loaded with the VEGF SmartFlares in combination with a fluorescent 10 kDa dextran to label fluid-phase endocytic pathways (A–C). After fixation, samples were immunostained either for the transferrin receptor (TFN-R: D–F) or lysosome-associated membrane protein 1 (LAMP1: G–I) to demark the recycling and lysosomal compartments respectively. Shown are SmartFlare fluorescence (A, D and G) and dextran or secondary antibody fluorescence (B, E and H). Panels (C, F and I) show an overlay of the two channels (SmartFlares pseudo-coloured red) with the Manders' coefficient (yellow number) expressing the proportion of SmartFlare Signal overlapping with the respective marker.

puncta (Figure 4B). There were approximately the same number of vesicles per cell when corrected for cell size. Interestingly, the dextran and SmartFlares rarely labelled the same compartments (Figure 4C) even at a 2-h time point (Figure S1).

As the dextran may be excluded from receptor-mediated endosomes (by unknown mechanisms) we also used immunofluorescence to label the recycling (transferrin-receptor positive) and terminal (lysosomal) compartments of the endocytic pathway (Figure 4D–F and G–I, respectively). Once again, the

SmartFlares showed little overlap with either of these compartments (Figure 4C, F and I, Manders' coefficients inset), suggesting a parallel but largely non-overlapping compartment.

CONCLUSIONS

Developing the green fluorescent protein into a tool for researchers was a landmark achievement across many fields and has opened up the dynamic study of proteins in living cells [26]. There is no doubt that replicating this success in the study of RNA would be equally as momentous. Our results, however, indicate that SNAs do not report on mRNA levels in live cells. Furthermore, we have shown that SNAs are taken up into only a subset of cells (which could potentially bias population studies). Once taken up we consistently observe a punctate distribution indicating retention within vesicular compartments. This was confirmed by electron microscopy and photothermal imaging. Furthermore, the controls (the scrambled and constitutively fluorescent uptake control) showed similar levels of fluorescence. As the fluorophore should only be dequenched in the presence of cognate mRNA, which we assume is not present in the vesicles, this signal is likely the result of a nucleolytic cleavage of the oligonucleotide strands. Indeed the Mirkin group themselves have published a comprehensive study on the vesicular retention and degradation of SNAs, particularly highlighting the role of DNaseII [27]. The same study highlights what an effective tool this must be if only a "…small, unquantifiable portion of these particles escape the endosome…" [27]. Even if we accept the possibility of a small fraction of these particles being released, unscathed into the cytosol, we still have the issue of overcoming background signal. StickyFlares (and presumably by extension, SmartFlares) are reported to increase in fluorescence intensity 10 times upon dequenching [15], which means that even if as many as 1 in 11 are released, the signal would not be visible over the background fluorescence. All of this is ignoring the cleavage and dequenching inside of the vesicle, which would further increase the background.

These findings leave us with the difficult job of interpreting the existing body of work published using these probes. It is likely that publication bias is playing a role: we do not know how many laboratories have bought and tried the SmartFlare reagents versus how many have published their results. Most of the published SmartFlare data are cytometry results which do not give any indication of the cellular localisation of the signal. Interestingly, when imaging data are included they show a punctate distribution in cells [28–30], although this is not commented upon. There have been other cases, most notably that of antisense technology, working but having an effect through means other than traditional Watson-Crick base pairing [31]. Thus, in addition to confirmation bias, some of the published work may result from poorly understood off-target effects.

REFERENCES

[1] Cruickshank J. The value and mechanism of the colloidal gold test. Br J Exp Pathol. 1920;1:71–88.

[2] Patterson J. The preparation and standardization of colloidal gold for the Lange test. Br J Exp Pathol. 1931;12:143–6.

[3] Harford CG, Hamlin A, Parker E. Electron microscopy of HeLa cells after the ingestion of colloidal gold. J Biophys Biochem Cytol. 1957;3 749–56.

[4] Epstein MA, Hummeler K, Berkaloff A. The entry and distribution of herpes virus and colloidal gold in HeLa cells after contact in suspension. J Exp Med. 1964;119:291–302.

[5] Maier O, Marvin SA, Wodrich H, Campbell EM, Wiethoff, CM. Spatiotemporal dynamics of adenovirus membrane rupture and endosomal escape. J Virol. 2012;86:10821–8. doi:10.1128/JVI.01428-12

[6] Bogart LK, Pourroy G, Murphy CJ, Puntes V, Pellegrino T, Rosenblum D, Peer D, Lévy R. Nanoparticles for imaging, sensing, and therapeutic intervention. ACS Nano. 2014;8:3107–22. doi:10.1021/nn500962q

[7] Iversen TG, Skotland T, Sandvig K. Endocytosis and intracellular transport of nanoparticles: present knowledge and need for future studies. Nano Today. 2011;6:176–85. doi:10.1016/j.nantod.2011.02.003

[8] Gilleron J, Querbes W, Zeigerer A, Borodovsky A, Marsico G, Schubert U, Manygoats K, Seifert S, Andree C, Stöter M, et al. Image-based analysis of lipid nanoparticle–mediated siRNA delivery, intracellular trafficking and endosomal escape. Nat Biotechnol. 2013;31:638–46. doi:10.1038/nbt.2612

[9] Varkouhi AK, Scholte M, Storm G, Haisma HJ. Endosomal escape pathways for delivery of biologicals. J Control Release. 2011;151:220–8. doi:10.1016/j.jconrel.2010.11.004

[10] Okada CY, Rechsteiner M. Introduction of macromolecules into cultured mammalian cells by osmotic lysis of pinocytic vesicles. Cell. 1982;29:33–41.

[11] Martens TF, Remaut K, Demeester J, De Smedt SC, Braeckmans K. Intracellular delivery of nanomaterials: how to catch endosomal escape in the act. Nano Today. 2014;9:344–64. doi:10.1016/j.nantod.2014.04.011

[12] Jun Y, Sheikholeslamia S, Hostetterb DR, Tajonb C, Craik CS, Paul Alivisatosa A. Continuous imaging of plasmon rulers in live cells reveals early-stage caspase-3 activation at the single-molecule level. Proc Natl Acad Sci U S A. 2009;106:17735–40. doi:10.1073/pnas.0907367106

[13] Zheng D, Seferos DS, Giljohann DA, Patel PC, Mirkin CA. Aptamer nano-flares for molecular detection in living cells. Nano Lett. 2009;9:3258–61. doi:10.1021/nl901517b

[14] Rosi NL, Giljohann DA, Thaxton CS, Lytton-Jean AK, Han MS, Mirkin CA. Oligonucleotide-modified gold nanoparticles for intracellular gene regulation. Science. 2006;312:1027–30. doi:10.1126/science.1125559

[15] Briley WE, Bondy MH, Randeria PS, Dupper TJ, Mirkin CA. Quantification and real-time tracking of RNA in live cells using Sticky-flares. Proc Natl Acad Sci U S A. 2015;112: 9591–5. doi:10.1073/pnas.1510581112

[16] Seferos DS, Giljohann DA, Hill HD, Prigodich AE, Mirkin CA. Nano-flares: probes for transfection and mRNA detection in living cells. J Am Chem Soc. 2007;129: 15477–9. doi:10.1021/ja0776529

[17] Mason D, Carolan G, Comenge J, Held M, Levy R. Posts about SmartFlare on Rapha-z-lab-commons [cite 2014 Sep]. Available from https://raphazlabcommons.wordpress.com/tag/smartflare/

[18] SmartFlares data repository [cite 2014 Sep]. Available from http://cci02.liv.ac.uk/gallery/show_project/1217/

[19] Nieves DJ, Li Y, Fernig DG, Lévy R. Photothermal raster image correlation spectroscopy of gold nanoparticles in solution and on live cells. R Soc Open Sci. 2015;2:140454. doi:10.1098/rsos.140454
[20] Bolte S, Cordelières FP. A guided tour into subcellular colocalization analysis in light microscopy. J Microsc. 2006;224: 213–32.
[21] Zhu T, Park HC, Son KM, Yang HC. Effects of dimethyloxalylglycine on wound healing of palatal mucosa in a rat model. BMC Oral Health. 2015;15: 60.
[22] Dehne N, Kerkweg U, Otto T, Fandrey J. The HIF-1 response to simulated ischemia in mouse skeletal muscle cells neither enhances glycolysis nor prevents myotube cell death. Am J Physiol Regul Integr Comp Physiol. 2007;293: R1693–701.
[23] EMD Millipore Bioscience. What if you could detect RNA in LIVING CELLS? 2014 [cite 2014 Sep]. Available from https://www.youtube.com/watch?v=CiSC2B8hl1E
[24] EMD Millipore Bioscience. SmartFlareTM Live Cell RNA Detection [cite 2014 Sep]. Available from http://www.merckmillipore.com/INTERSHOP/web/WFS/Merck-GB-Site/en_US/-/GBP/ViewParametricSearch-SimpleOfferSearch?search=&SearchTerm=smartflare
[25] Herrmann A, Rice M, Lévy R, Pizer BL, Losty PD, Moss D, Sée V. Cellular memory of hypoxia elicits neuroblastoma metastasis and enables invasion by non-aggressive neighbouring cells. Oncogenesis. 2015;4: e138. doi:10.1038/oncsis.2014.52
[26] Enterina JR, Wu L, Campbell RE. Emerging fluorescent protein technologies. Curr Opin Chem Biol. 2015;27: 10–17. doi:10.1016/j.cbpa.2015.05.001
[27] Wu XA, Choi CHJ, Zhang C, Hao L, Mirkin CA. Intracellular fate of spherical nucleic acid nanoparticle conjugates. J Am Chem Soc. 2014;136:7726–33. doi:10.1021/ja503010a
[28] Lahm H, Doppler S, Dreßen M, Werner A, Adamczyk K, Schrambke D, Brade T, Laugwitz KL, Deutsch MA, Schiemann M, et al. Live fluorescent RNA-based detection of pluripotency gene expression in embryonic and induced pluripotent stem cells of different species. Stem Cells. 2015;33:392–402. doi:10.1002/stem.1872
[29] Kratz A, Beguin P, Kaneko M, Chimura T, Suzuki AM, Matsunaga A, Kato S, Bertin N, Lassmann T, Vigot R, et al. Digital expression profiling of the compartmentalized translatome of Purkinje neurons. Genome Res. 2014;24:1396–410.
[30] Krönig M, Walter M, Drendel V, Werner M, Jilg CA, Richter AS, Backofen R, McGarry D, Follo M, Schultze-Seemann W, et al. Cell type specific gene expression analysis of prostate needle biopsies resolves tumor tissue heterogeneity. Oncotarget. 2015;6:1302–14.
[31] Raffo A. Antisense RNA down-regulation of bcl-2 expression in DU145 prostate cancer cells does not diminish the cytostatic effects of G3139 (Oblimersen). Clin Cancer Res. 2004;10:3195–206.

COMPETING INTERESTS

The authors declare no competing interests.

PUBLISHING NOTES

Please note that this article may not have been peer reviewed yet and is under continuous post-publication peer review. For the current reviewing status please click **here** or scan the QR code on the right.

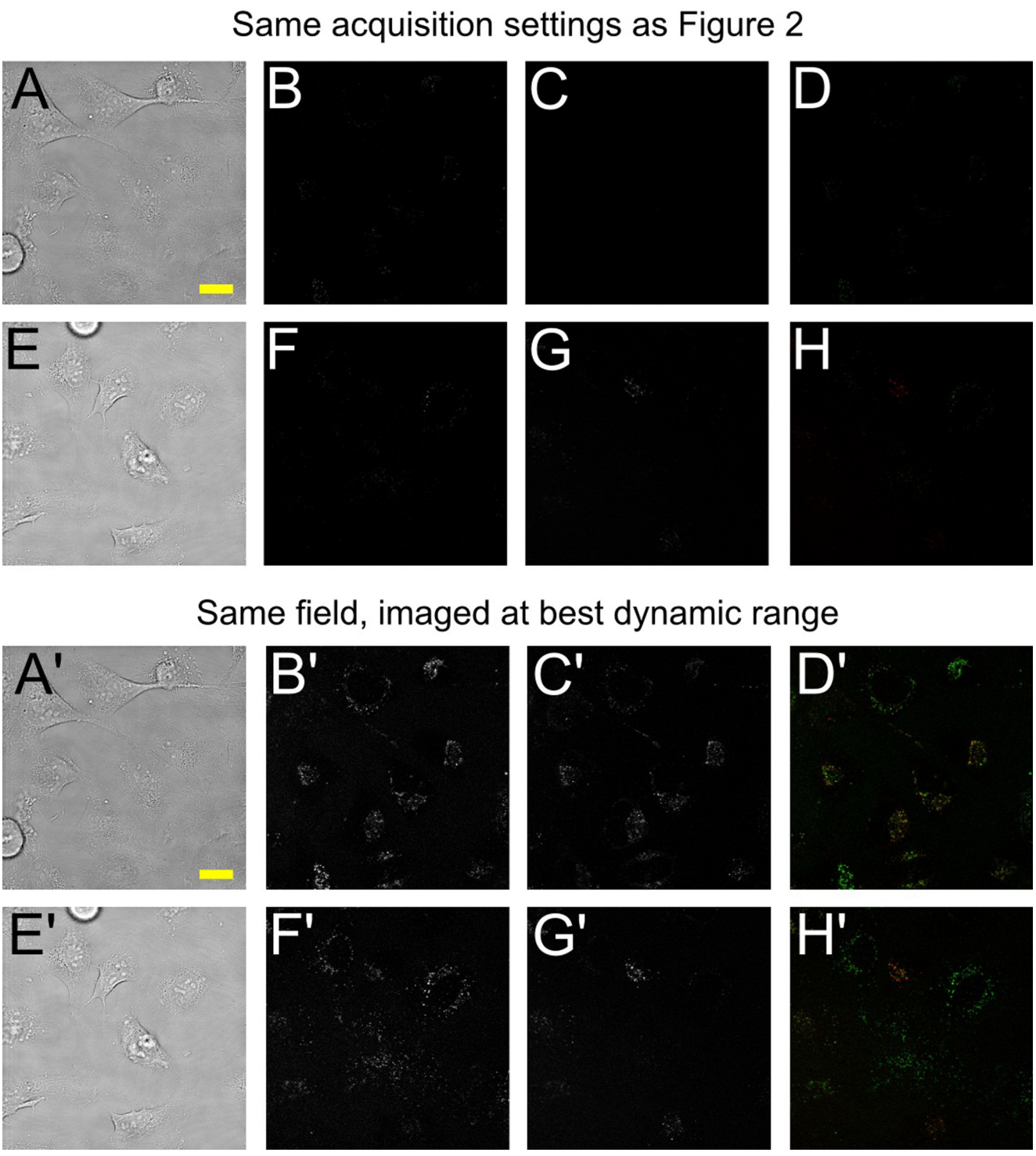

Supplementary Figure S1. SmartFlare uptake at 2 h: HeLa cells were exposed to uptake control (A–D) or VEGF (E–H) SmartFlares for 2 h, then washed and imaged with confocal laser-scanning microscopy in fluorescence (B, C, F and G) or transmitted (A and E) channels. An overlay of the SmartFlares (pseudo-coloured red) and Dextran (pseudo-coloured green) is shown in D and H. The top panels (A–H) show the same imaging parameters as were used for 18-h experiments. The bottom panels (A′–H′) show the identical field imaged with optimal dynamic range for visualisation. All frames are shown at identical magnification, scale bar represents 20 µm.